

# **Soft Matter**

# Hydrophobic Fouling-Resistant Electrospun Nanofiber Membranes from Poly(vinylidene fluoride)/Polyampholyte Blends

Journal:	Soft Matter		
Manuscript ID	SM-ART-07-2024-000817.R1		
Article Type:	Paper		
Date Submitted by the Author:	07-Oct-2024		
Complete List of Authors:	Jayasekara, Anuja; Tufts University, Physics and Astronomy Mazzaferro, Luca; Tufts University, Chemical and Biological Engineering O'Hara, Ryan; Tufts University, Chemical and Biological Engineering Asatekin, Ayse; Tufts University, Department of Chemical & Biological Engineering Cebe, Peggy; Tufts University, Physics and Astronomy		

SCHOLARONE™ Manuscripts

# Hydrophobic Fouling-Resistant Electrospun Nanofiber Membranes from Poly(vinylidene fluoride)/Polyampholyte Blends

Anuja S Jayasekara<sup>1</sup>, Luca Mazzaferro<sup>2</sup>, Ryan O'Hara<sup>2</sup>, Ayse Asatekin<sup>2</sup>, Peggy Cebe<sup>1</sup>

 $^{\rm 1}\, {\rm Department}$  of Physics & Astronomy

<sup>2</sup> Department of Chemical & Biological Engineering

Tufts University, Medford MA 02155

Contact Information: peggy.cebe@tufts.edu

Soft Matter Page 2 of 29

#### **Abstract**

This study reports the fabrication of non-woven fibrous membranes from electrospinning blended solutions of PVDF with polyampholytes in N,N-dimethylformamide and methanol. Polyampholytes are macromolecules that have both positive and negative charged units in different side groups attached to the backbone. In this study, we used a random polyampholyte amphiphilic copolymer (r-PAC) synthesized by co-polymerizing a hydrophobic monomer in addition to the positive and negative charged monomer units, to reduce the fouling propensity of PVDF electrospun membranes while preserving its inherent hydrophobicity. Blends of PVDF/r-PAC were electrospun across the full range of compositions from 0/100 to 100/0. Scanning electron microscopic analysis showed formation of beaded fibers with average fibril diameters from 0.09 μm - 0.18 μm. The variation in the fiber diameters is caused by the change in surface charge density, dynamic viscosity of the solution, and the instability of the Taylor cone. Bead formation was observed in the mats electrospun from less viscous solutions. Wide angle X-ray scattering showed that electrospun fibers of PVDF crystallized into the electro-active  $\beta$  and  $\gamma$  crystal phases, whereas polyampholytes were amorphous. Thermogravimetry showed that the PVDF/r-PAC blends have a multi-step thermal degradation mechanism while PVDF homopolymer showed single-step thermal degradation. Sessile drop contact angle measurements confirmed that fibers possess high hydrophobicity and super-oleophilicity. Adsorptive fouling experiments with a fluorescently labeled protein confirmed that the fiber mats obtained from the PVDF/r-PAC blends resist protein adsorption, exhibiting highly enhanced fouling resistance compared to the fibers obtained from homopolymer PVDF.

Page 3 of 29 Soft Matter

## 1. Introduction

Membrane filtration is an energy-efficient, simple, compact process for many purification challenges, from removing bacteria and other microorganisms to generate safe drinking water to wastewater treatment to the purification of biologic drugs <sup>1,2</sup>. Poly(vinylidene fluoride), PVDF, is a highly preferred material for membrane filters due to its chemical and physical stability, mechanical strength, and processability. However, its high hydrophobicity leads to membrane fouling <sup>3-5</sup>, which affects the life span of the filtration membrane by reducing the flux significantly and adding to the operational costs <sup>6-8</sup>. Several methods exist for improving the fouling resistance of a membrane.

One of the most efficient methods of making a membrane fouling-resistant is increasing its surface hydrophilicity <sup>6, 9</sup>. Blending PVDF with hydrophilic materials including polymers and nanoparticles, and surface modification of PVDF membranes by grafting or coating hydrophilic segments, are broadly studied techniques directed toward improving its hydrophilicity <sup>6, 8</sup>. Blending mechanisms have significant advantages such as allowing convenient operation from fewer number of steps <sup>10, 11</sup>, improving the hydrophilicity in the whole membrane matrix instead of only the surface, and cost effectiveness <sup>12</sup>. In addition, unlike surface modification <sup>11</sup>, blending techniques do not affect the porosity of the membrane. Successful polymer additives for decreasing fouling in membranes are often amphiphilic, with hydrophobic segments anchoring hydrophilic, anti-fouling groups or brushes to the surface of the membrane <sup>13, 14</sup>. In this work, we use polyampholytes blended with PVDF to decrease membrane fouling.

Polyampholytes are defined as polymers that comprise anionic and cationic groups in different monomer units on the same chain. Polyampholytic materials can prevent fouling of surfaces by the adsorption of proteins and other organic macromolecules. This is believed to be due, in part, Soft Matter Page 4 of 29

to a strong hydration shell layer created by the charged groups on the polymer chain <sup>15-18</sup>. Leng, et al.19 state that the hydration layer on the surface is tightly bound to the surface by electrostaticinduced hydrogen bonding between water molecules and ether oxygen atoms. Because of this strong attachment, the hydration layer acts as a physical barrier as well as an energy barrier for biomolecular foulants such as proteins. Yet, there are only a few previous reports of polyampholytes being used to enhance fouling resistance on commercial membrane surfaces <sup>20, 21</sup> . Recently, Mazzaferro, et al. <sup>22</sup> introduced a family of novel amphiphilic polyampholyte copolymers that could be coated on a porous support to serve as the "selective layer" of membranes with tunable selectivity and remarkable fouling resistance. These polymers were designed to be insoluble in water to avoid dissolution during use and comprised three types of monomers: a hydrophobic monomer to provide stability, and the combination of an anionic and a cationic monomer to create the ampholytic, fouling-resistant behavior as well as enable water permeation. However, to our knowledge, there are no reports of blending amphiphilic polyampholytes to a commodity polymer (e.g., PVDF) during manufacturing to create more fouling-resistant membranes.

Non-woven fibrous membranes can be obtained by the process of electrospinning. Electrospinning is an efficient method to obtain nanoscale fibers<sup>23</sup> which show excellent surface area-to-volume ratios and enhanced porosity, making make them good options for liquid filtration mechanisms <sup>23-25</sup>. Non-woven fibrous membranes help overcome some of the limitations found in non-fibrous membranes in filtration applications, such as lower mechanical stress and non-uniform pore distribution <sup>23</sup>. PVDF is a widely used polymer in electrospinning applications as well <sup>26-29</sup>. Electrospun PVDF membranes are already in extensive use in filtration applications <sup>25, 27, 30-32</sup> such as air-borne particle filtration<sup>33</sup>, heavy metal filtration<sup>34</sup>, and oil-water filtration<sup>7</sup>. Blends of PVDF

Page 5 of 29 Soft Matter

with various copolymers have been used to create electrospun mats with improved filtration capabilities, including but not limited to zwitterionic copolymers for enhanced organic fouling resistance, or fluorinated copolymers for high hydrophobicity and selective oil permeation <sup>27, 35, 36</sup>. However, polyampholytes are not often used as electro-spinnable materials. To the best of our knowledge, only two groups reported on electrospinning of polyampholytes <sup>37, 38</sup>. Mincheva, et al. <sup>37</sup> report electrospinning a variety of polyampholytes in combination with non-ionogenic polymers to associate and stabilize the electrospinning process.

In this study, we electrospun nanofiber membranes from PVDF and its blends with a random polyampholyte amphiphilic copolymer (r-PAC) containing methacrylic acid, and [2-(methacryloyloxy)-ethyl]trimethylammonium chloride, and 2,2,2-trifluoroethyl methacrylate. This r-PAC is similar to the one used by Mazzaferro, et al. <sup>22</sup> as self-assembled membrane selective layers shown to have remarkable fouling resistance. Despite the similarity of its chemical structure, the hydrophobic TFEMA units are not fully miscible with PVDF due to the repulsive dipolar interactions between fluorine atoms in both polymer chains <sup>39</sup>. As a result, PVDF and the r-PAC incorporating these hydrophobic units had to be dissolved in a mixture of dimethylformamide (DMF) and methanol to ensure good solubility. The membranes were characterized using scanning electron microscopy (SEM), wide angle X-ray scattering (WAXS), thermogravimetric (TG) analysis, and sessile drop contact angle measurements. The fouling resistance was documented using a common protein foulant, bovine serum albumin (BSA) tagged with fluorescein isothiocyanate (FITC) for visualization.

# 2. Experimental Section

2.1 Synthesis of Poly(2,2,2-trifluoroethylmethacrylate)-random-poly[2-(methacryloyloxy)ethyl]-trimethylammoniumchloride)-random-poly(methacrylic acid)

Soft Matter Page 6 of 29

A random terpolymer with three monomeric units was synthesized using methacrylic acid (MAA, Sigma Aldrich), [2-(methacryloyloxy)ethyl]trimethylammonium chloride (MAETA, Sigma Aldrich), and 2,2,2-trifluoroethyl methacrylate (TFEMA, ACROS Organics). The first two monomers were passed through a column of neutral activated alumina (Sigma Aldrich) to remove the inhibitor, while the last monomer was passed through a column of basic activated alumina (VWR). MAA (1.46 g, 17.0 mmol), MAETA (3.54 g, 17.0 mmol), and 2,2,2-trifluoroethyl methacrylate (5.00 g, 29.7 mmol) were dissolved in this order in dimethyl sulfoxide (DMSO, 40 mL, Fisher). Azobisisobutyronitrile (AIBN, 0.01 g, Sigma Aldrich) was added to the flask. The flask was sealed with a rubber septum. Nitrogen was bubbled through the reaction mixture for 30 min to purge any dissolved oxygen. The flask was then kept at 60 °C while stirring at 300 rpm for 17 h. After the reaction, 1 g of 4-methoxyphenol (MEHQ, Sigma Aldrich) was added to terminate the synthesis. The reaction mixture containing DMSO and the polymer was poured in 600 mL of acetone to precipitate the polymer. After the removal of the precipitation solvent the polymer was washed by stirring two fresh portions of 1:3 ethanol to hexane volume ratio for at least 5 h, and two fresh portions of acetone for at least 5 h; all portions were around 500 mL. Finally, the terpolymer was dried in a vacuum oven for 72 h at 60 °C. The composition of the terpolymer was calculated from the <sup>1</sup>H-NMR spectrum (**Fig. 1**), using the ratio of protons from the three different monomer units. The calculated composition was: 25 mol% MAA, 25 mol% MAETA, and 50 mol% TFEMA. The final conversion of this reaction was 57%.

Page 7 of 29 Soft Matter

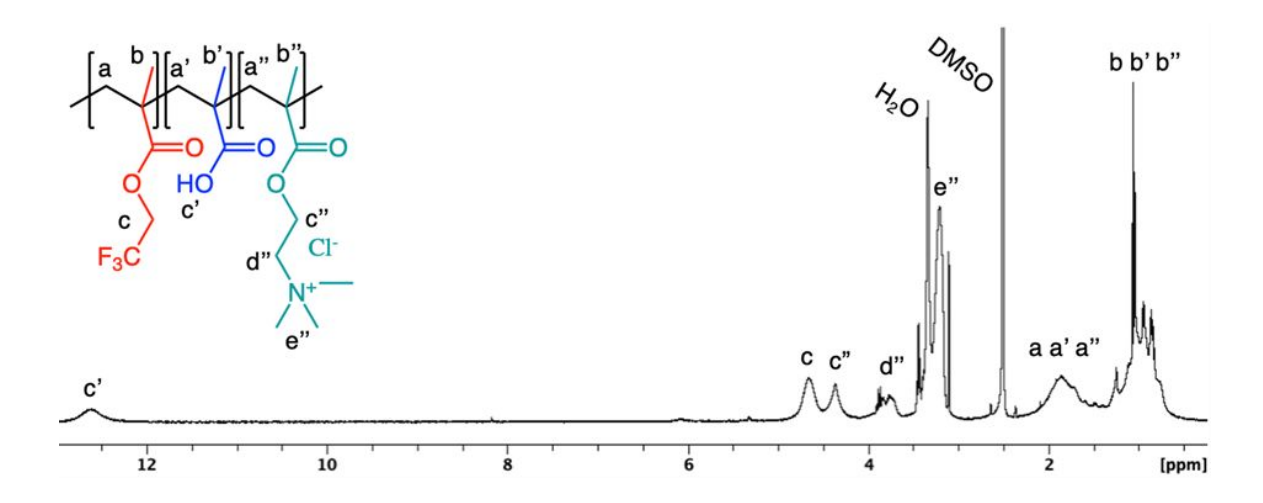


**Figure 1.** NMR spectrum of r-PAC chemical structure indicating copolymerization of the three monomer units. Inset shows the structure of r-PAC. The subgroups are: TFEMA (red, left); MAA (blue, middle); MAETA (green, right).

## 2.2 Materials

PVDF powder (KYNAR® grade 301F) was kindly provided by Arkema Chemicals, Inc. (King of Prussia, PA, USA). Phosphate buffered saline (PBS) powder was purchased from Thermo Fisher Scientific (Waltham, MA, USA) and used after mixing with ultra-pure DI water as instructed by the recipe, resulting in a pH 7.4 solution. Albumin from Bovine Serum (BSA), fluorescein isothiocyanate conjugate (FITC-BSA) was purchased from Thermo Fisher Scientific (Waltham, MA, USA). (N,N-dimethylformamide (DMF) and methanol (MeOH) from Oakwood Products Inc (Estill, SC, USA) were used as-received. PVDF and r-PAC powders were mixed in the following ratios (PVDF/r-PAC): 100/00, 95/05, 90/10, 75/25, 50/50, 25/75, and 00/100 in a way that the total polymer concentration is 10 wt.% in DMF/MeOH (13/01 v/v). A short label format is used to

Soft Matter Page 8 of 29

identify the samples with different ratios. For example, PVDF/r-PAC 75/25 sample is labelled as PVDF75.

# 2.3 Electrospinning

Prepared solutions were drawn into a glass syringe (internal diameter 14.67 mm) and mounted on a syringe pump system (NE-1000 New Era Pump Systems Inc. Farmingdale, NY, USA). An 18-gauge steel needle (inner diameter 0.84 mm) was attached to the syringe. A collector plate (diameter of 25 cm) rotating at angular speed of 1 rpm and wrapped in Aluminum foil was used to collect fibers. The applied voltage and the working distance between the needle tip and the collector plate varied between 25 kV - 27.5 kV and 15 cm - 22.5 cm, respectively. The solution was pumped at a flow rate between 0.5 mL/h - 1.0 mL/h. These variables were adjusted to address the variation of the viscosity of the solution and the subtle changes in the relative humidity of the atmosphere. Examples of the obtained electrospun fiber mats, and the electrospinning set up, are shown in Fig. 2.

## 2.4 Characterization Methods

Scanning electron microscopic (SEM) analysis was performed on small pieces cut from the obtained fiber mats. The pieces were mounted on standard SEM stubs with conducting carbon tape. Au/Pd (60/40) was plasma deposited using a Cressington 108 Manual sputter coater (Ted Pella Inc., CA, USA) on the samples to view them under SEM at an increased resolution. A Phenom Delphi SEM (Eindhoven, Netherlands) operated at 10 kV was used to observe the surface morphology of the fibers. The average diameter of the fibers was determined by using the DiameterJ plugin available on ImageJ which is public domain software. A detailed description of the fiber diameter analysis, and the method for removal of the beads, is provided in Appendix A: Supplementary Data.

Page 9 of 29 Soft Matter

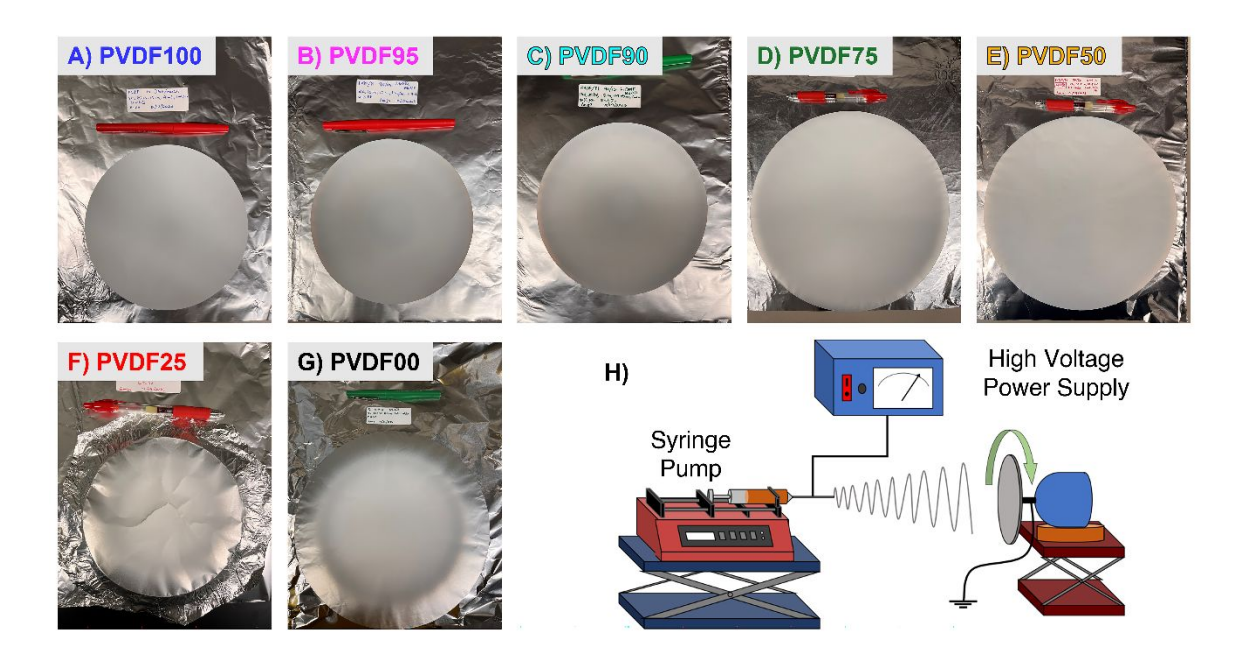


**Figure 2.** Optical images of electrospun fiber mats of: A) PVDF100; B) PVDF95; C) PVDF90; D) PVDF75; E) PVDF50; F) PVDF25; G) PVDF00; H) Schematic of the electrospinning setup, showing syringe pump, high voltage source, fiber whipping, and rotating grounded collector plate from Govinna <sup>40</sup>. A pen (~15 cm) is used to indicate the scale in A-G.

Wide angle X-ray scattering intensity (WAXS) vs. scattering angle,  $2\theta$ , was obtained for all electrospun mats using a Philips PW 1830 X-ray generator (Panalytical, Almelo, Netherlands). The system provided nickel filtered Cu K<sub> $\alpha$ </sub> radiation of wavelength,  $\lambda = 0.154$  nm, operated at 30 kV and 55 mA at room temperature, with a diffracted beam graphite monochromator. All samples were mounted on Al sample holders and scans were obtained in  $\theta/2\theta$  reflection mode. WAXS intensity plots were recorded at a step scan interval of 0.02 °/step with a dwell time of 2 s/step. The scattering angle varied from 5° - 40°.

Soft Matter Page 10 of 29

Thermogravimetric (TG) analysis was conducted on all samples using a TGA Q500 (TA Instruments, New Castle, DE, USA) to determine the thermal degradation properties. The samples were heated at a rate of 10 °C/min from 25 °C -600 °C with a dry nitrogen purge of 50 mL/min. The sample mass varied from 3 mg -10 mg. All TG tests were performed by placing the samples directly on a clean Pt basket. To determine the degradation onset temperatures, the intersection point of the extrapolated line in the dry undegraded states, and the tangent line drawn along the degradation step was used. We recorded the degradation onset temperature with an uncertainty of  $\pm 1$  °C.

Sessile drop contact angle measurements were performed on all samples using a contact angle goniometer (Ramé-Hart Instrument Co., NJ, USA) with water and dodecane, an oil-like hydrocarbon liquid, to determine, respectively, the hydrophilic (or hydrophobic) and oleophilic (or oleophobic) surface wetting properties. Five droplets of water and oil were placed at different locations on each sample to determine the average contact angle. All contact angle values are reported with an uncertainty of  $\pm$  3°.

Fouling samples were prepared by punching out circular samples (10 mm diameter) from electrospun fiber mats adhered to aluminum foil. These samples were attached to a 35 mm polystyrene petri dish with double-sided tape, which was filled with 5 mL of phosphate buffered saline (PBS) and kept covered to prepare the sample surface for protein fouling. After 1 h, the PBS was removed, and 5 mL of a 0.1 mg/mL solution of FITC-BSA in PBS was added. Samples were kept in the dark to reduce photobleaching and moved to an oven at 37°C for 1.5 h. The FITC-BSA solution was then removed and replaced with fresh PBS 3 times, followed by soaking the samples in fresh PBS for 15 min on a rocker plate 3 more times. The samples were then washed once with DI water to reduce PBS crystallization during imagining. Background samples were also prepared

Page 11 of 29 Soft Matter

following the same protocol; however, these samples did not come into contact with the FITC-BSA solution. Epifluorescence micrographs of the fouled electrospun fibers were obtained using an Olympus BX51 microscope (Olympus Corp., Center Valley, PA, USA) equipped with a DP70 microscope digital camera, 10x objective lens, and a standard green (U–N31001) filter set (Chroma Technology Corp., Rockingham, VT, USA). Exposure was optimized to be 1/5 sec to prevent background signal and pixel intensity overflow. Relative fluorescence intensity was calculated using ImageJ's mean grey value function on each image of the fouled and unfouled samples and calculated using Equation 1. The sample background intensity was subtracted from the fouled sample intensity, normalized to the difference between the PVDF100 fouled sample and background intensities, and converted to a percent.

Relative Fluorescence Intensity (%) = 
$$\frac{I_{Sample Fouled} - I_{Sample Background}}{I_{PVDF100 Fouled} - I_{PVDF100 background}} * 100\%$$
 (1)

## 3. Results and Discussion

SEM images obtained for each sample are shown in **Fig. 3** (A-G). As evident in Fig. 3G, homopolymer r-PAC was successfully electrospun to form fibrous membranes with an average fiber diameter of  $0.28~\mu m \pm 0.19~\mu m$ . To the best of our knowledge, this is the first time a polyampholyte has been electrospun to obtain fibers without incorporating another polymer to stabilize the electrospinning process. The fibers contain a significant number of beads. The shape of the beads is more spherical when the PVDF fraction is high. This is caused by the low viscosity of the solutions with higher PVDF contents and as a result some electrospraying could occur. On the other hand, when the r-PAC fraction becomes greater the solution viscosity is increased significantly, and the beads become elongated and form along with the fibers. The presence of beads is rare in the PVDF50 electrospun mat. The average diameter of the fibers obtained for all

Soft Matter Page 12 of 29

samples was estimated using the DiameterJ plugin in the ImageJ application. **Table 1** reports the average fibril diameter after exclusion of the beads, in comparison to the average bulk fiber diameter including the beads. After exclusion of the beads, PVDF75 and PVDF50 showed the two smallest fibril diameter values of  $0.09 \pm 0.02 \mu m$  and  $0.12 \pm 0.03 \mu m$ , respectively. (see Supplementary Data S1, **Fig.S1** (A-G) for histograms of the fiber diameter distributions).

As shown in Fig. 3-H, the average fibril diameter initially decreases from PVDF100 to PVDF75 with the addition of r-PAC and then increases again from PVDF50 to PVDF00. Fiber diameter can be affected by several different parameters of the electrospinning process and by the properties of the polymer solution. Electrospinning processing variables include deposition rate (or, the pumping speed), Taylor cone stability, and the applied voltage. The effect of electrospinning parameters on the fiber diameter is a widely studied area as the diameters of the fibers produced by electrospinning are distributed over a wide range<sup>41-46</sup>. According to Cramariuc, et al.<sup>42</sup> and Fridrikh, et al.<sup>43</sup>, the terminal diameter of the polymer jet that eventually determines the fiber diameter is controlled by the deposition rate, electric current due to bulk motion of surface charges in the polymer solution and conduction through the solution<sup>44</sup>, and the surface tension of the solution.

During electrospinning, the pumping rate was varied. PVDF100 solution was pumped at 1 mL/hr and the rest of the solutions were pumped at 0.5 – 0.6 mL/hr because the applied electric field was too weak to form a stable jet when electrospinning PVDF/r-PAC blends and homopolymer r-PAC. The variation of deposition rate might be one reason for the gradual reduction of fibril diameters observed from PVDF100 to PVDF75.

Properties of the solutions also affect the fiber diameters. For example, surface charge density and conductivity of the polymer fluid, which directly influences the electric current of the polymer jet,

Page 13 of 29 Soft Matter

has an inverse effect on fiber diameter, as discussed by Cramariuc, et al.<sup>42</sup> and Fridrikh, et al.<sup>43</sup>. As the fraction of r-PAC is increased the fiber diameter decreases because the surface charge density and conductivity of the solution increase with the introduction of the ionic r-PAC units. The applied electric field also affects the electric current, but the variations we made in the working distance and the applied voltage make the variations in the electric field negligible.

As shown in Fig. S6 in Appendix A: Supplementary Data, the dynamic viscosity and the average fibril diameters show an inverse relationship between them. Addition of r-PAC to the solution increases the dynamic viscosity of the solution first, and then as the r-PAC fraction increases and starts to dominate, the viscosity begins to decrease. Accordingly, as r-PAC fraction increases, the average fibril diameter first decreases and then starts to increase again. The low viscosity of the solutions with high r-PAC fractions such as PVDF25 and PVDF00 may have caused the bead formation observed in their respective fiber mats. It is observed that the Taylor cone was slightly unstable when electrospinning PVDF25 and PVDF00. The Taylor cone was periodically varying its size during the electrospinning process which could be another cause why PVDF25 and PVDF00 exhibited beading in the fibers as Singh, et al.<sup>45</sup> state that the instabilities of the Taylor cone have a complex effect on the fiber diameters.

Soft Matter Page 14 of 29

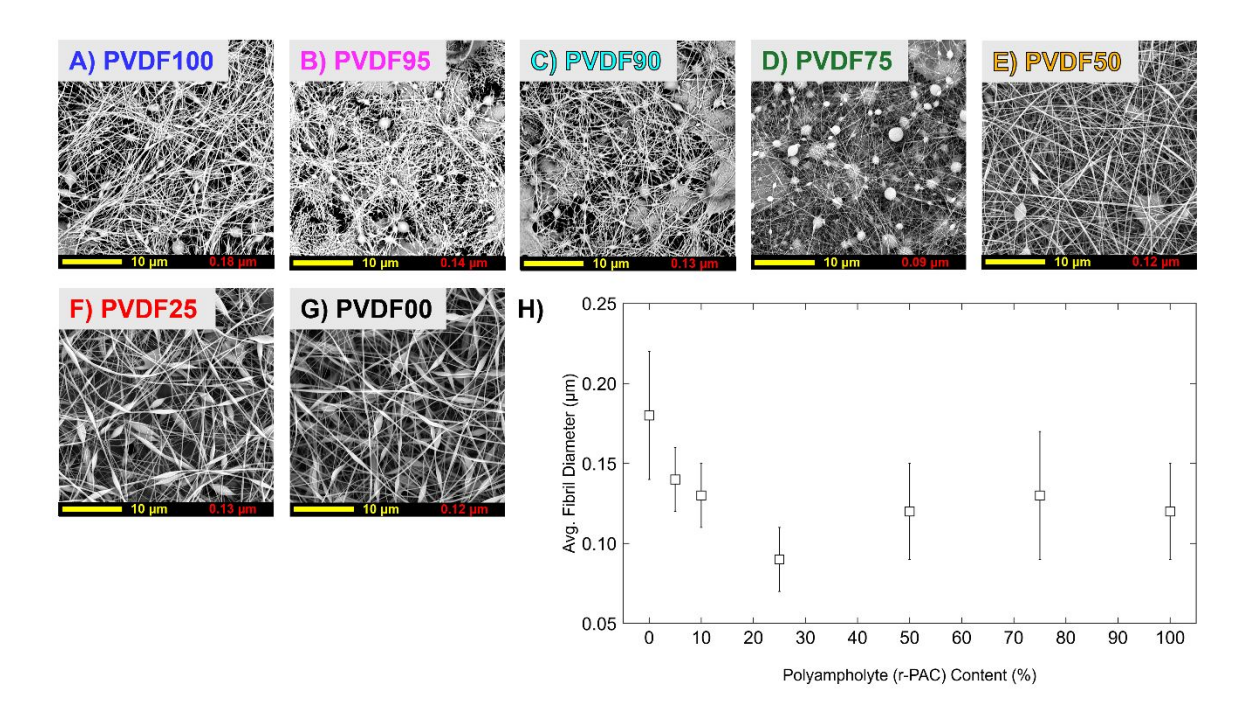


**Figure 3.** SEM images of the electrospun fibers. A) PVDF100; B) PVDF95; C) PVDF90; D) PVDF75; E) PVDF50; F) PVDF25; G) PVDF00; H) Variation of fibril diameters in all electrospun mats. All images were obtained at a magnification of 7500x and scale bars are 10 μm. Average fibril diameter is shown on each image at the lower right.

The porosity of each fibrous mat was also estimated using DiameterJ. As shown in **Table 1**, PVDF75 and PVDF50 showed the two smallest mean pore areas  $0.26 \pm 0.02 \,\mu\text{m}^2$  and  $0.27 \pm 0.01 \,\mu\text{m}^2$ , respectively. PVDF75 and PVDF50 also showed the two highest pore densities  $14.0 \times 10^5 \, \text{mm}^{-2}$  and  $15.3 \times 10^5 \, \text{mm}^{-2}$ , respectively. About 75% of the pores in each sample had areas below the mean pore area indicating high porosity with smaller pore sizes.

Page 15 of 29 Soft Matter

**Table 1:** Average diameters and pore data of electrospun fibers of PVDF/r-PAC Blends

	Average Bulk	Average Fibril	Mean Pore	Pore Density d
Sample Name	Fiber Diameter a	Diameter <sup>b</sup>	Area <sup>c</sup>	
	(µm)	(µm)	$(\mu m^2)$	$(\times 10^5  \text{mm}^{-2})$
PVDF00	$0.27 \pm 0.18$	$0.12 \pm 0.03$	$0.72 \pm 0.03$	6.35
PVDF25	$0.25 \pm 0.17$	$0.13 \pm 0.04$	$0.48 \pm 0.02$	8.62
PVDF50	$0.20 \pm 0.11$	$0.12 \pm 0.03$	$0.27 \pm 0.01$	15.3
PVDF75	$0.17 \pm 0.14$	$0.09 \pm 0.02$	$0.26 \pm 0.02$	14.0
PVDF90	$0.29 \pm 0.17$	$0.13 \pm 0.06$	$0.49 \pm 0.04$	6.95
PVDF95	$0.29 \pm 0.15$	$0.14 \pm 0.02$	$0.46 \pm 0.03$	6.06
PVDF100	$0.28 \pm 0.14$	$0.18 \pm 0.04$	$0.43 \pm 0.02$	8.13

<sup>&</sup>lt;sup>a</sup> Bulk diameter includes the beads – See Appendix A: Supplementary Data for description of this calculation

**Fig. 4** shows the WAXS intensity vs. scattering angle of all samples. PVDF00 (bottom, black) shows a broad peak centered at 16.5° (dotted purple line) and none of the narrow intense peaks characterizing a crystalline material. This confirms that homopolymer r-PAC was not able to form any crystalline domains due to its bulky structure and lack of stereoregularity. However, a narrow intense peak emerges around  $20^{\circ}$ – $21^{\circ}$  as the PVDF fraction increases (from PVDF25 to PVDF100). This peak is a convolution of two peaks centered at  $20.4^{\circ}$  ( $d_{021}^{\gamma} = 0.431$  nm – long-dashed purple line) and  $20.7^{\circ}$  ( $d_{200/110}^{\beta} = 0.427$  nm – short-dashed purple line) which correspond, respectively, to the  $\gamma$ - and  $\beta$ -crystallographic phases of PVDF  $^{47,48}$ . These two phases,  $\gamma$  and  $\beta$ , are the electroactive (EA) phases of PVDF  $^{26,29,49}$ , hence the presence of EA crystal phases in the electrospun fiber mats is confirmed. Electrospinning is known to produce EA crystal phases of PVDF as it simultaneously applies electrical and mechanical forces to stretch the polymer chain  $^{50}$ . The absence of the triplet of peaks between  $25^{\circ}$  -  $30^{\circ}$  (at  $25.8^{\circ}$  ( $d_{120}^{\alpha} = 0.344$  nm),  $26.7^{\circ}$  ( $d_{021}^{\alpha}$ 

<sup>&</sup>lt;sup>b</sup> Fibril diameter does not include the beads – See Appendix A: Supplementary Data for description of this calculation

The nine images shown in Fig. S1 were examined for pores and the average number of pores per image is listed in Table S1. The magnification of the images was the same for all samples.

<sup>&</sup>lt;sup>d</sup> SEM images were converted from pixel units to mm<sup>2</sup>.

Soft Matter Page 16 of 29

= 0.334 nm), and 28.1° ( $d_{111}^{\alpha}$  = 0.318 nm)) in all samples confirms that there are no  $\alpha$ -phase crystals in any of the electrospun fiber samples <sup>48,51</sup>.

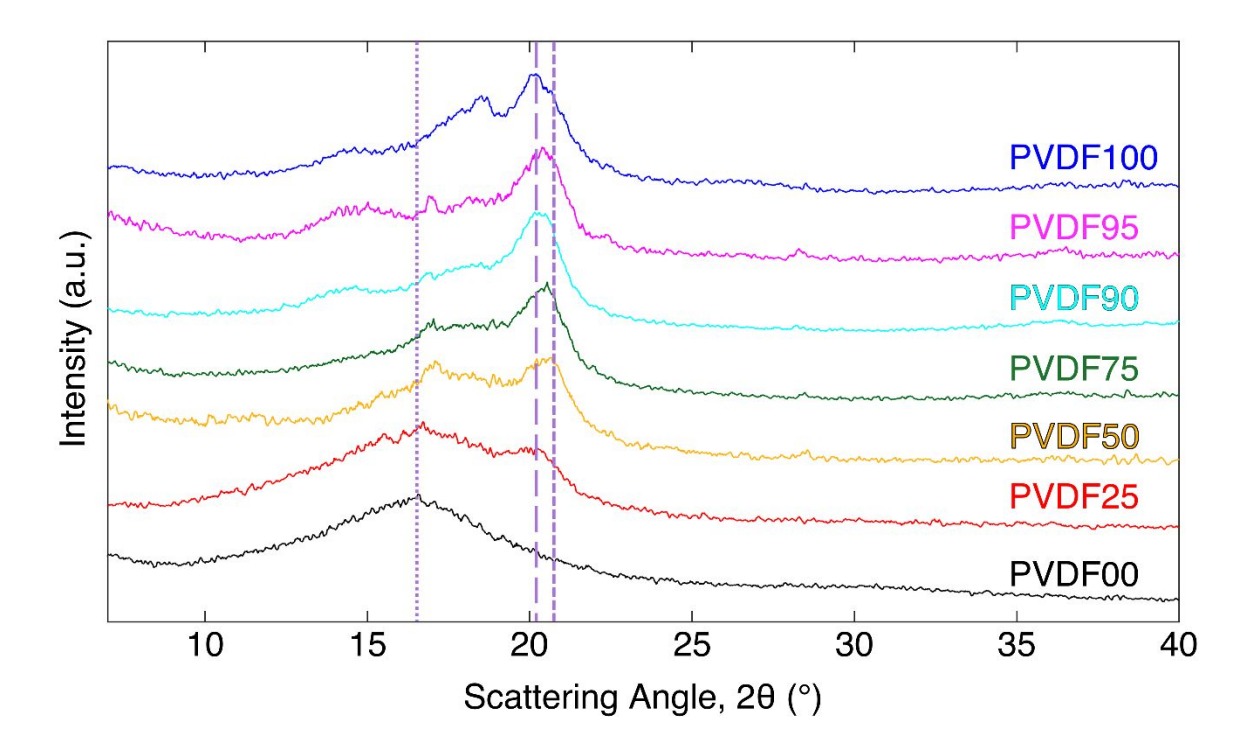


**Figure 4.** WAXS intensity vs. scattering angle of: PVDF100 (homopolymer PVDF, top, blue); PVDF95 (magenta); PVDF90 (cyan); PVDF75 (green); PVDF50 (yellow); PVDF25 (red); PVDF00 (r-PAC, bottom, black). The vertical purple lines show the scattering angle at the following reflections: r-PAC amorphous halo (dotted line);  $\gamma$ -phase reflection (long-dashed line);  $\beta$ -phase reflection (short-dashed line).

**Fig. 5** shows the results of thermogravimetric (TG) analysis of each sample. Homopolymer PVDF sample, PVDF100 (top, blue), shows excellent thermal stability with only one degradation onset point around 450 °C which is typical for PVDF <sup>35</sup>. Homopolymer r-PAC (bottom, black) and its blends with PVDF show complex TG curves with multiple degradation steps. The blends show thermal stability up to 180 °C and their first significant mass loss occurs from 180 °C to 200 °C. A second mass loss can be seen from 240 °C to 250 °C, followed by a third degradation step, which

Page 17 of 29 Soft Matter

can be seen around 400 °C. Goel, et al. <sup>52</sup> and Shukla, et al. <sup>53</sup> report that pMAETA possess super hygroscopic properties. Hence, the initial mass loss at lower temperatures which is evident in r-PAC and its blends with PVDF can be accounted for by ejection of the bound water.

At temperatures above the ejection of bound water, the observed degradation steps in the blends containing r-PAC correspond to the degradation of charged side groups in the r-PAC. Supeno, et al. <sup>54</sup> and Goel, et al. <sup>52</sup> reported that polymerized MAETA (pMAETA) (the positively charged side group in r-PAC) degrades around 230 °C and 400 °. Ho, et al. <sup>55</sup>, Bajaj, et al. <sup>56</sup>, and McNeil, et al. <sup>57</sup> report that polymerized MAA (pMAA) (negatively charged side group in r-PAC) also shows a two-step degradation process comprising a first step around 200 °C – 230 °C and a second step around 400 °C. Polymerized TFEMA is reported to have a significant mass loss around 360 °C – 400 °C according to Xu, et al. <sup>58</sup>, Fang, et al. <sup>59</sup>, and Li, et al <sup>60</sup>. The blends also show a fourth degradation step at 450 °C which is caused by the degradation of the PVDF component.

Soft Matter Page 18 of 29

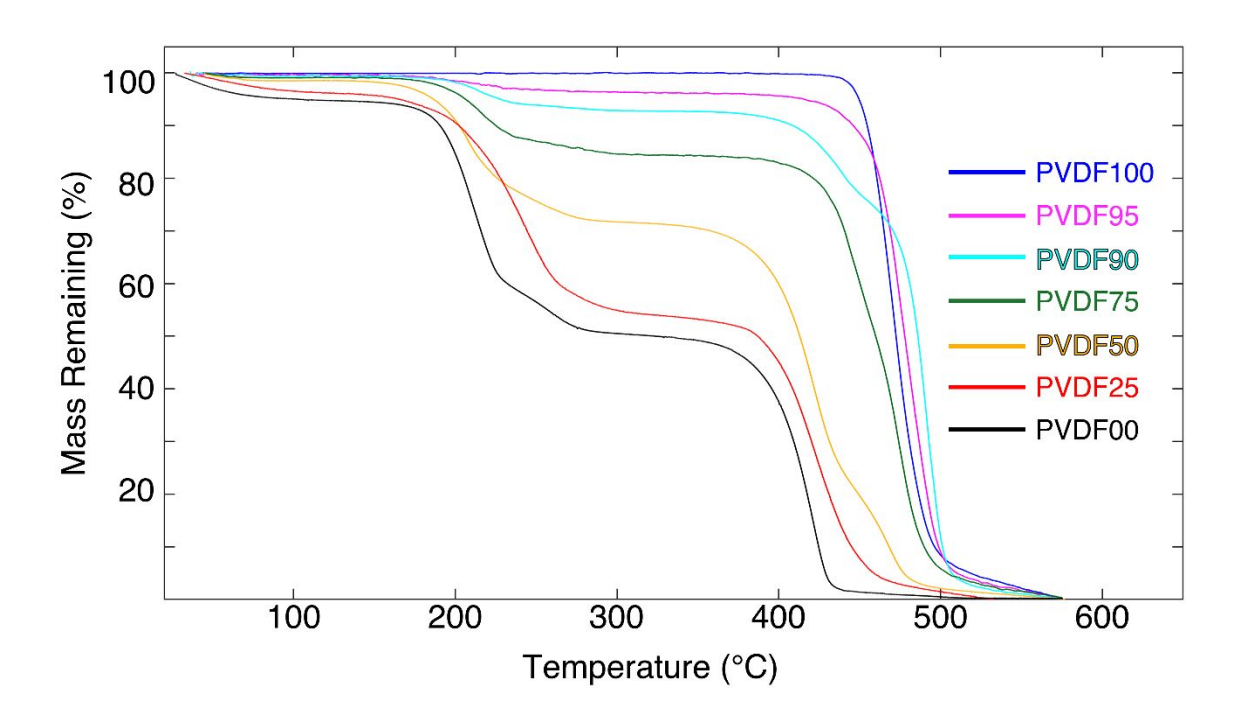


**Figure 5.** Thermogravimetric analysis showing the remaining mass fraction vs. temperature for: PVDF100 (top, blue); PVDF95 (magenta); PVDF90 (cyan); PVDF75 (green); PVDF50 (yellow); PVDF25 (red); PVDF00 (bottom, black). The initial mass loss for temperatures below 100 °C is due to bound water ejection. The r-PAC homopolymer and its blends with PVDF show multiple thermal degradation steps whereas homopolymer PVDF show single-step thermal degradation.

The sessile drop contact angle measurements conducted with water on all samples are shown in **Fig. 6**. PVDF100 fibers exhibited a water contact angle of 128°, indicating a significant increase in hydrophobicity compared to its thin film form, which has a contact angle of 95° <sup>61, 62</sup>. This is obvious because the fibers of a material have a higher surface area-to-volume ratio which leads to a higher surface energy compared to the material's thin film form. PVDF95 and PVDF90 show no significant change in the contact angle with water compared to PVDF100. Their contact angles

Page 19 of 29 Soft Matter

were 127° and 129°, respectively. However, when the PVDF content drops to 75% or less (r-PAC content 25% or greater), the contact angle increases to 136° indicating a significant increase in hydrophobicity as the hydrophobic content increases drastically as TFEMA (the hydrophobic unit in r-PAC) fraction in the fibers rise and the fiber diameters rapidly decrease. The contact angle maintains this higher value and does not vary significantly with further increase of r-PAC content. The highest contact angle was observed for PVDF00 (the homopolymer r-PAC), with a value of 139° - a substantial increase from its thin film form, which had a contact angle of 82°. Hence, all electrospun fibrous mats are very hydrophobic.

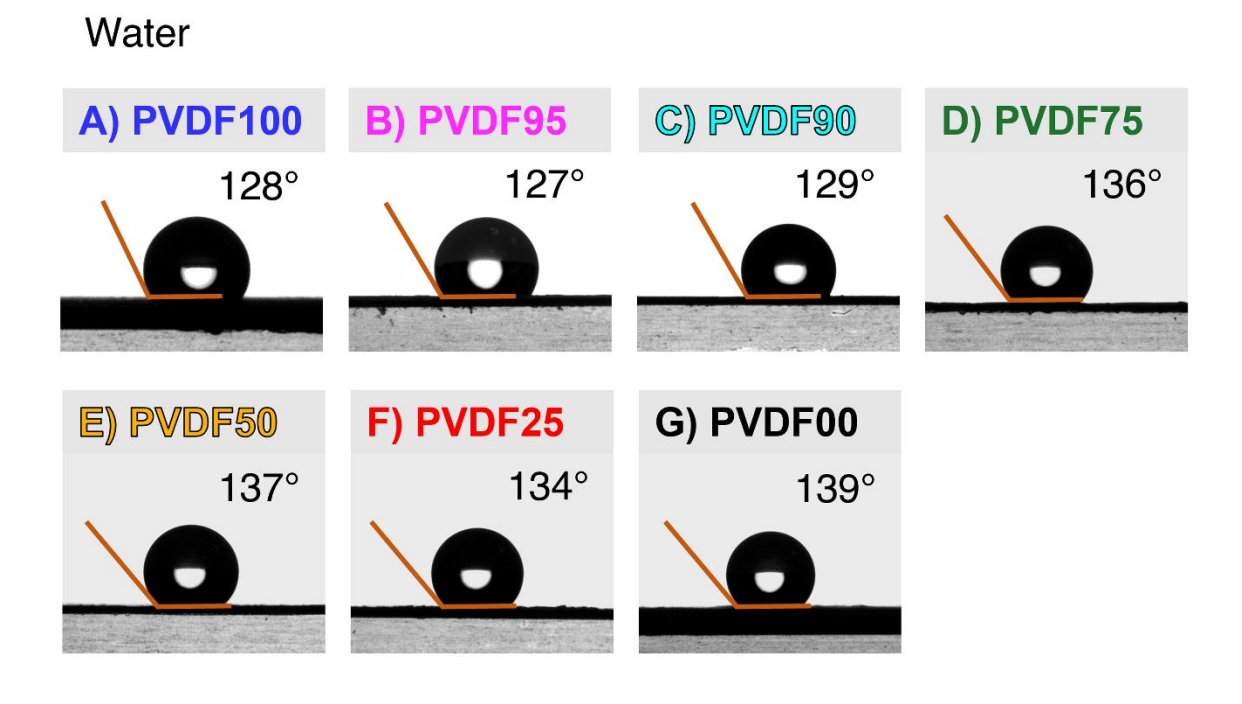


**Figure 6.** Sessile drop contact angle measurements for a water droplet on electrospun fiber mats of: A) PVDF100; B) PVDF95; C) PVDF90; D) PVDF75; E) PVDF50; F) PVDF25; G) PVDF00 at room temperature (25 °C). The water droplet is shown by the black orb and the angle between the orange lines indicates the contact angle. The measured values are shown on each figure.

Soft Matter Page 20 of 29

The contact angle measurements were also taken using dodecane, an oil-like substance, and are presented in Supplementary Data S3 videos A-G. All fibrous mats showed very small contact angles indicating that they are super-oleophilic. The oil droplets dispersed over the surface of the fibrous mats within seconds after deposition. This implies that the electrospun fiber mats would be well suited for applications in oil/water separation, where oil is selectively absorbed into the mat.

Proteins are one of the most significant biomacromolecular foulants found in many water and wastewater treatment applications, and are often used as key probes for testing fouling resistance. Therefore, to quantify the fouling resistance of PVDF/r-PAC electrospun mats, we performed static adsorption experiments of a common, highly fouling protein, bovine serum albumin (BSA), labeled with the fluorescent dye fluorescein isothiocyanate (FITC). Each electrospun mat was immersed in a solution of this labeled protein, FITC-BSA, for 1.5 h. After rinsing to remove any unbound protein, the mats were imaged using fluorescence microscopy to determine how much protein remained adsorbed to the surface (Fig. 7). Total fluorescence intensity in each image, quantified by image analysis, is correlated with the amount of FITC-BSA. The pure PVDF mat, PVDF100, exhibited the highest protein adsorption, and was thus used as the reference material for calculating differences in fouling propensity. Therefore, "relative fluorescence intensity" was defined to indicate the amount of protein adsorbed on each mat normalized by the amount on PVDF100 (Equation 1). All PVDF/r-PAC samples, PVDF95, PVDF90, PVDF75, PVDF50, and PVDF25, as well as PVDF00, showed a significant decrease in fluorescence intensity of at least 50% (Fig. 7H). PVDF50, PVDF25, and PVDF00 showed a relative fluorescence intensity of less than 10%, indicating that despite being hydrophobic, these electrospun mats have excellent fouling resistance and can resist nearly all protein adsorption.

Page 21 of 29 Soft Matter

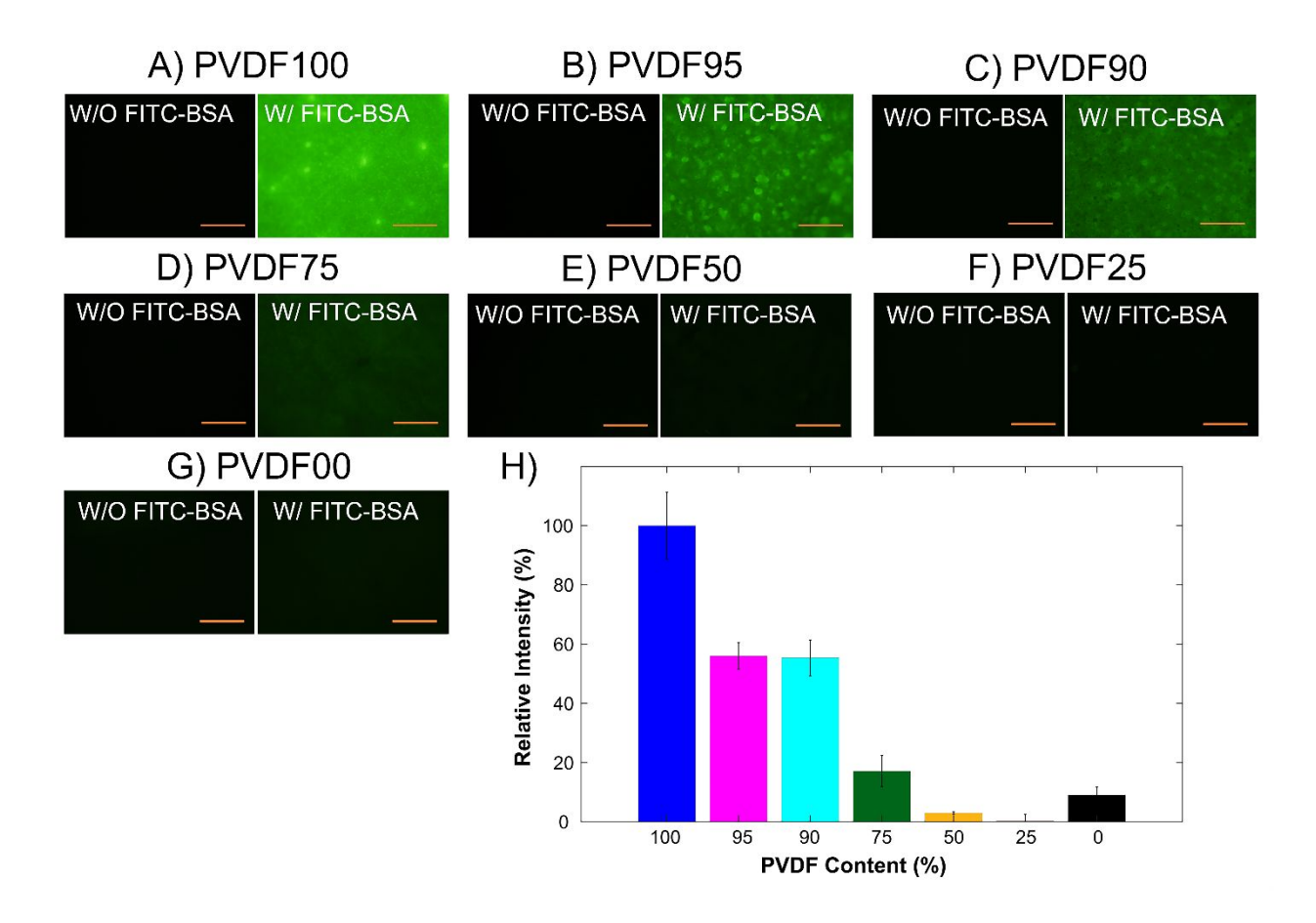


**Figure 7.** A-G) Epifluorescence micrographs of electrospun fiber mats after fouling with the fluorescently labeled protein FITC-BSA (W/FITC-BSA) on the right sides, compared with images of mats that were not exposed to the protein as a control (W/O FITC-BSA) on the left sides. Scale bars are 200 μm. Selected micrographs are representative images of the whole sample. H) Relative extent of protein adsorption reported as relative fluorescence intensity compared to fouled pure PVDF samples. Fluorescence intensity, which is proportional to the amount of adsorbed protein, was quantified by calculating the mean grey value for each image in ImageJ and normalized with the extent of fouling of PVDF samples (Eqn. 1). At least 4 randomly selected images were taken per mat. Error bars were calculated using propagation of uncertainty.

Soft Matter Page 22 of 29

#### 4. Conclusions

In this article, we report successful use of electrospinning to obtain fibrous membranes of a random polyampholyte ter-copolymer (r-PAC) and its blends with PVDF. The average diameter of homopolymer r-PAC fibrils was 0.12 µm. Fibers made from blends with PVDF also had submicron scale fibrils, with minimum diameter (0.09 µm) occurring in PVDF75. Fiber formation was enhanced with increasing r-PAC fraction. Minimal beading was seen in PVDF50, i.e., when PVDF and r-PAC were blended in equal parts. The average fibril diameters showed an inverse relationship with the solution viscosity. The solution viscosity increased as the r-PAC content was raised, peaking in PVDF75, after which the viscosity began to decrease. On the other hand, the fibril diameter first decreased and then increased for compositions beyond PVDF75. The mean pore area also showed a variation similar to that of fiber diameters with increasing r-PAC fraction. Higher pore densities were observed in PVDF75 and PVDF50 compared to the other electrospun mats because of small fibril diameters and reduced tendency for beading.

While all the blends of PVDF/ r-PAC and the homopolymer PVDF crystallized into the electroactive (EA) crystal phases as detected in WAXS, homopolymer r-PAC was completely amorphous. The TG curves showed that PVDF/r-PAC blends and homopolymer r-PAC are thermally stable below 180 °C. Above 180 °C, the blends and homopolymer r-PAC show a complex multi-step thermal degradation process whereas homopolymer PVDF showed excellent thermal stability up to 450 °C.

The sessile drop contact angle measurements showed that fibrous mats obtained from all materials, including homopolymer r-PAC and PVDF, and all PVDF/r-PAC blends, are very hydrophobic with contact angles over 120° with water. However, they showed very low contact angles with dodecane (oil) and the oil droplets were immediately dispersed on the surface after deposition

Page 23 of 29 Soft Matter

confirming that the mats are super-oleophilic. These properties confirm that electrospun fibers of

PVDF/r-PAC may be ideal materials for oil-water filtration.

The addition of r-PAC to PVDF led to significant, even drastic, decreases in protein adsorption

when the r-PAC content was 25% or greater. This indicates that, in addition to being highly

hydrophobic, these materials are highly resistant to fouling by biomacromolecular solutes.

In summary, our findings in this study highlight the applications of r-PAC and its blends with

PVDF as potential materials for wastewater treatment processes displaying high hydrophobicity

and excellent fouling resistance over a broad composition range. In a future study, we will report

on the thermal properties of these materials such as their heat capacities and melting behavior.

5. Acknowledgements

The authors thank the National Science Foundation (NSF) Division of Materials Research,

Polymers Program, for support of this research through the Grant DMR-2003629. The authors

thank Prof. Hyunmin Yi of the Department of Chemical and Biological Engineering at Tufts

University for access to the epifluorescence microscopy facility.

**Appendix A: Supplementary Data** 

23

Soft Matter Page 24 of 29

# References

- 1. J. Cevallos-Mendoza, C. G. Amorim, J. M. Rodríguez-Díaz and M. d. C. B. Montenegro, Membranes, 2022, **12**, 570.
- 2. S. Hube, M. Eskafi, K. F. Hrafnkelsdóttir, B. Bjarnadóttir, M. Á. Bjarnadóttir, S. Axelsdóttir and B. Wu, Science of the total environment, 2020, **710**, 136375.
- D. Wanke, A. da Silva and C. Costa, Chemical Engineering Research and Design, 2021,
  171, 268-276.
- 4. L. Wang, R. Miao, X. Wang, Y. Lv, X. Meng, Y. Yang, D. Huang, L. Feng, Z. Liu and K. Ju, Environmental Science & Technology, 2013, 47, 3708-3714.
- 5. G.-d. Kang and Y.-m. Cao, Journal of membrane science, 2014, **463**, 145-165.
- S. Madaeni, S. Zinadini and V. Vatanpour, Journal of membrane science, 2011, 380, 155-162.
- 7. S. Gopi, R. Kargl, K. S. Kleinschek, A. Pius and S. Thomas, Journal of environmental management, 2018, **228**, 249-259.
- 8. L. N. Nthunya, L. Gutierrez, L. Lapeire, K. Verbeken, N. Zaouri, E. N. Nxumalo, B. B. Mamba, A. R. Verliefde and S. D. Mhlanga, Separation and Purification Technology, 2019, 228, 115793.
- 9. Y. S. Li, L. Yan, C. B. Xiang and L. J. Hong, Desalination, 2006, **196**, 76-83.
- 10. F. Liu, N. A. Hashim, Y. Liu, M. M. Abed and K. Li, Journal of membrane science, 2011, 375, 1-27.
- H. Younas, Y. Zhou, X. G. Li, X. Li, Q. Y. Sun, Z. L. Cui and Z. H. Wang, Polymer, 2019,
  179, 9.

Page 25 of 29 Soft Matter

12. C. N. B. Elizalde, S. Al-Gharabli, J. Kujawa, M. Mavukkandy, S. W. Hasan and H. A. Arafat, Separation and Purification Technology, 2018, **190**, 68-76.

- 13. A. Asatekin, S. Kang, M. Elimelech and A. M. Mayes, Journal of Membrane Science, 2007, **298**, 136-146.
- 14. P. Kaner, A. V. Dudchenko, M. S. Mauter and A. Asatekin, Journal of materials chemistry A, 2019, 7, 4829-4846.
- 15. J. Ladd, Z. Zhang, S. Chen, J. C. Hower and S. Jiang, Biomacromolecules, 2008, 9, 1357-1361.
- M. Bernards and Y. He, Journal of Biomaterials Science, Polymer Edition, 2014, 25, 1479-1488.
- 17. S. C. Dobbins, D. E. McGrath and M. T. Bernards, The Journal of Physical Chemistry B, 2012, **116**, 14346-14352.
- 18. C. A. Del Grosso, C. Leng, K. Zhang, H.-C. Hung, S. Jiang, Z. Chen and J. J. Wilker, Chemical Science, 2020, 11, 10367-10377.
- 19. C. Leng, H.-C. Hung, S. Sun, D. Wang, Y. Li, S. Jiang and Z. Chen, ACS applied materials & interfaces, 2015, 7, 16881-16888.
- A. P. Straub, E. Asa, W. Zhang, T. H. Nguyen and M. Herzberg, Chemical Engineering Journal, 2020, 382, 122865.
- 21. W. Zhang, Z. Yang, Y. Kaufman and R. Bernstein, Journal of colloid and interface science, 2018, **517**, 155-165.
- L. Mazzaferro, S. J. Lounder and A. Asatekin, ACS Applied Materials & Interfaces, 2023,
  15, 42557-42567.

Soft Matter Page 26 of 29

- 23. T. He, W. Zhou, A. Bahi, H. Yang and F. Ko, Chemical Engineering Journal, 2014, 252, 327-336.
- Z. Zhao, J. Zheng, M. Wang, H. Zhang and C. C. Han, Journal of membrane science, 2012,
  394, 209-217.
- Y. Liao, C.-H. Loh, M. Tian, R. Wang and A. G. Fane, Progress in Polymer Science, 2018,
  77, 69-94.
- 26. E. S. Cozza, O. Monticelli, E. Marsano and P. Cebe, Polymer International, 2013, **62**, 41-48.
- N. Govinna, P. Kaner, D. Ceasar, A. Dhungana, C. Moers, K. Son, A. Asatekin and P. Cebe, Polymer International, 2019, 68, 231-239.
- 28. L. Yu and P. Cebe, Polymer, 2009, **50**, 2133-2141.
- 29. A. S. Jayasekara and P. Cebe, Polymer, 2023, 126140.
- 30. R. Roche and F. Yalcinkaya, Nanomaterials, 2018, **8**, 771.
- 31. C. Feng, K. Khulbe, T. Matsuura, S. Tabe and A. F. Ismail, Separation and purification technology, 2013, **102**, 118-135.
- 32. S. A. A. N. Nasreen, S. Sundarrajan, S. A. Syed Nizar, R. Balamurugan and S. Ramakrishna, Polymer journal, 2014, **46**, 167-174.
- 33. A. Sanyal and S. Sinha-Ray, Polymers, 2021, **13**, 1864.
- 34. M. Salehi, D. Sharafoddinzadeh, F. Mokhtari, M. S. Esfandarani and S. Karami, 2021.
- 35. N. Govinna, I. Sadeghi, A. Asatekin and P. Cebe, Journal of Polymer Science Part B: Polymer Physics, 2019, **57**, 312-322.
- 36. I. Sadeghi, N. Govinna, P. Cebe and A. Asatekin, ACS Applied Polymer Materials, 2019,1, 765-776.

Page 27 of 29 Soft Matter

37. R. Mincheva, N. Manolova, D. Paneva and I. Rashkov, Journal of bioactive and compatible polymers, 2005, **20**, 419-435.

- 38. Q. Wang, University of Missouri--Columbia, 2014.
- 39. D. Jouannet, T.-N. Pham, S. Pimbert and G. Levesque, Polymer, 1997, **38**, 5137-5147.
- 40. N. D. Govinna, Tufts University, 2019.
- 41. V. Beachley and X. Wen, Materials Science and Engineering: C, 2009, 29, 663-668.
- 42. B. Cramariuc, R. Cramariuc, R. Scarlet, L. R. Manea, I. G. Lupu and O. Cramariuc, Journal of Electrostatics, 2013, **71**, 189-198.
- 43. S. V. Fridrikh, J. H. Yu, M. P. Brenner and G. C. Rutledge, Physical review letters, 2003, **90**, 144502.
- 44. M. M. Hohman, M. Shin, G. Rutledge and M. P. Brenner, Physics of fluids, 2001, **13**, 2221-2236.
- 45. S. K. Singh and S. Sarma, Journal of Electrostatics, 2022, **120**, 103770.
- 46. X. Yan and M. Gevelber, Particulate Science and Technology, 2017, **35**, 139-149.
- 47. L. Yu and P. Cebe, Journal of Polymer Science Part B: Polymer Physics, 2009, **47**, 2520-2532.
- 48. B. S. Ince-Gunduz, K. Burke, M. Koplitz, M. Meleski, A. Sagiv and P. Cebe, Journal of Macromolecular Science, Part A: Pure and Applied Chemistry, 2010, 47, 1208-1219.
- 49. C. Fu, H. Zhu, N. Hoshino, T. Akutagawa and M. Mitsuishi, Langmuir, 2020, **36**, 14083-14091.
- 50. W. A. Yee, M. Kotaki, Y. Liu and X. Lu, Polymer, 2007, 48, 512-521.
- 51. B. S. Ince-Gunduz, R. Alpern, D. Amare, J. Crawford, B. Dolan, S. Jones, R. Kobylarz, M. Reveley and P. Cebe, Polymer, 2010, **51**, 1485-1493.

Soft Matter Page 28 of 29

- 52. N. Goel, M. Rao, V. Kumar, Y. Bhardwaj, C. Chaudhari, K. Dubey and S. Sabharwal, Radiation Physics and Chemistry, 2009, **78**, 399-406.
- 53. N. B. Shukla, R. K. Bhagat and G. Madras, Polymer-Plastics Technology and Engineering, 2013, **52**, 58-65.
- 54. Supeno, R. Daik and S. M. El-Sheikh, 2014.
- 55. B. C. Ho, Y. D. Lee and W. K. Chin, Journal of Polymer Science Part A: Polymer Chemistry, 1992, **30**, 2389-2397.
- 56. P. Bajaj, M. Goyal and R. Chavan, Journal of applied polymer science, 1994, **51**, 423-433.
- 57. I. McNeill and J. Liggat, Polymer degradation and stability, 1992, **36**, 291-299.
- 58. A.-h. Xu, L.-q. Zhang, J.-c. Ma, Y.-m. Ma, B. Geng and S.-x. Zhang, Journal of Coatings Technology and Research, 2016, **13**, 795-804.
- 59. J. Fang, H. Xu, X. Wei, M. Guo, X. Lu, C. Lan, Y. Zhang, Y. Liu and T. Peng, Polymers for advanced technologies, 2013, 24, 168-173.
- 60. G. Li, A. Xu, B. Geng, S. Yang, G. Wu and S. Zhang, Journal of Fluorine Chemistry, 2014, **165**, 132-137.
- 61. A. Wang, M. Shao, F. Yang, C. Shao and C. Chen, European Polymer Journal, 2021, **160**, 110803.
- 62. E. Fontananova, M. Bahattab, S. Aljlil, M. Alowairdy, G. Rinaldi, D. Vuono, J. Nagy, E. Drioli and G. Di Profio, RSC Advances, 2015, **5**, 56219-56231.

Page 29 of 29 Soft Matter

# **Data Availability Statement**

Data for this article are available at Harvard Dataverse, including Metadata and MATLAB codes, at <a href="https://doi.org/10.7910/DVN/HLNEGN">https://doi.org/10.7910/DVN/HLNEGN</a> and <a href="https://doi.org/10.5281/zenodo.12636577">https://doi.org/10.5281/zenodo.12636577</a>, respectively.